JMEPEG (2007) 16:680–684
DOI: 10.1007/s11665-007-9099-y

1059-9495/$19.00

Microstructures and Mechanical Properties Prediction for Ti-Based Alloys

Jianzheng Guo and Mark T. Samonds

(Submitted May 10, 2006; in revised form November 22, 2006)

Titanium alloys have been used in demanding applications such as the chemical industry and aerospace, thanks to their excellent corrosion resistance, low density, and high-mechanical strength. There have been many research activities recently on titanium alloys, mainly focusing on experiments. The kinetics of phase transformations and the relationship between the microstructure and the final mechanical properties has not been widely studied by computer modeling. In this work, a comprehensive finite-element model coupled with thermodynamic calculations has been developed to simulate the microstructure evolution and predict the final mechanical properties resulting from solidification and β to α solid phase transformation. This model can be applied to casting and heat treatment processes. The predictions are validated by comparison with experimental measurements. The results show that this model can accurately predict the microstructure, volume fraction of different phases, and the final yield strength of titanium alloys.

Keywords casting, heat treatment, mechanical properties, microstructure, modeling, titanium

1. Introduction

The improvement of alloy properties relies on an accurate prediction of the microstructure during solidification, defect formation, and the microstructure evolution during solid phase transformations, as might occur from heat treatment (Ref 1). The mechanical properties are very much dependent on the microstructure, which are determined by the alloy chemistry and the applied processes. Hence it is very important to understand the thermodynamics and kinetics of the alloy during its phase changes. There are three types of microstructures for titanium alloys: α, α + β, and β. The types of phases present, the volume fraction of the phases, grain size, and grain shape determine the properties, which in turn govern the appropriate applications of the alloy (Ref 2). The bcc β-phase {110} can transform to the basal planes {0001} of the hexagonal α-phase under some conditions. The distance between the basal planes in α is slightly larger than the corresponding distance between the {110} planes in β. The growth of the α-phase in a supersaturated β matrix is diffusion controlled. This transformation process can be described by some partial differential equations.

Although the strengthening mechanisms in Ni-based, Al-based, and Fe-based alloys are well known and characterized by mathematical relationships, the exact relationships between microstructural features and the mechanical properties of Ti-based alloys are still not clear. There have been many experimental works to study the microstructure evolution for α + β Ti-based alloy castings (Ref 3-7), heat treatment (Ref 8-10), and thermomechanical processing (Ref 11-17). Some modeling works on the β to α-phase transformation can been found in the literature (Ref 2, 14). In this work, a solidification model is presented first. Then a computer model is developed to predict the nucleation and growth of α-phase during solid cooling processes. The grain size and volume fraction of different phases can be predicted. Finally, the mechanical properties are calculated based upon the simulated microstructure.

Jianzheng Guo and **Mark T. Samonds,** ESI US R&D, 5850 Waterloo Road, suite 140, Columbia, MD 21045. Contact e-mail: jianzhengguo@gmail.com.

2. Solidification Modeling

Simulation technologies are applied extensively in casting industries to understand the aspects of heat transfer and fluid transport phenomena and their relationships to the microstructure and the formation of defects (Ref 1). Microstructure during solidification of alloys is a very important factor for the control of the properties and the quality of casting products (Ref 18). Thermodynamic calculations are coupled with the macro-scale thermal and fluid flow calculations.

The nucleation is based on the model proposed by Thevoz and co-workers (Ref 18) which is illustrated in Fig. 1. At a given undercooling, the grain density n is calculated by the integral of the nucleation site distribution from zero undercooling to the current undercooling.

The density of grain nuclei can be written as:

$$n(\Delta T(t)) = \frac{n_{\max}}{\sqrt{2\pi}\cdot\Delta T_\delta}\int_0^{\Delta T(t)} \exp\left(-\frac{(\Delta T(t)-\Delta T_n)^2}{2\Delta T_\sigma^2}\right) d(\Delta T(t)), \quad \text{(Eq 1)}$$

where $n_{\max}$: maximum grain nuclei density; ΔT_δ: standard deviation undercooling; and ΔT_n average undercooling.

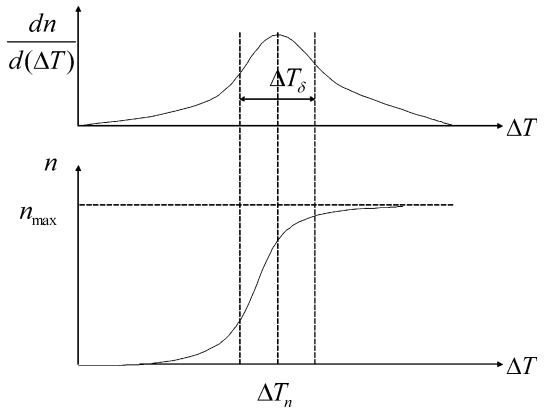

Fig. 1 Nucleation model

Rappaz and Boettinger (Ref 19) studied the growth of an equiaxed multicomponent dendrite. In their study, for each element, the supersaturation is

$$\Omega_j = \frac{c^*_{l,j} - c_{o,j}}{c^*_{l,j}(1-k_j)} = Iv(Pe_j), \quad \text{(Eq 2)}$$

where $J = 1$, n solute element; $c_{l,j}{}^*$: tip liquid concentration; $c_{o,j}$: nominal concentration; and k_j: partition coefficient.

Pe is call Peclet number and defined as: $Pe_j = \frac{Rv}{2D_j}$, where D_j is the diffusion coefficient.

The Ivanstsov function is defined as: $Iv(Pe) = Pe \cdot \exp(Pe) \cdot E_1(Pe)$, where E_1 (Pe) is the first exponential integral.

Assuming growth at the marginal stability limit, the dendrite radius is calculated by

$$R = \frac{-2\pi^2\Gamma}{\sum_{j=1}^{n} m_j Pe_j \frac{c_{o,j}(1-k_j)}{1-(1-k_j)Iv(Pe_j)}}, \quad \text{(Eq 3)}$$

where Γ is the Gibbs-Thomson coefficient.

Hence the tip velocity can be derived:

$$v = D_1 Pe_1 \frac{2}{R} \quad \text{(Eq 4)}$$

and the tip liquid concentration will be:

$$c^*_{l,j} = \frac{c_{o,j}}{1-(1-k_j)Iv(Pe_j)}. \quad \text{(Eq 5)}$$

Assume that the liquid concentration in the inter-dendritic region is uniform. The solute profiles in the extradendritic liquid region can be obtained from an approximate model (Ref 20)

$$J_j = D_j \cdot \left(\frac{c^*_{l,j} - c_{o,j}}{\delta_j/2}\right), \quad \text{(Eq 6)}$$

where the solute layer thickness is:

$$\delta_j = \frac{2D_j}{v}. \quad \text{(Eq 7)}$$

So the solute balance will become:

$$\frac{df_s}{dt}\sum_{j=1}^{n} m_j(k_j-1)c^*_{l,j} + (f_g - f_s)\frac{dT}{dt} - \sum_{j=1}^{n} m_j J_j = 0, \quad \text{(Eq 8)}$$

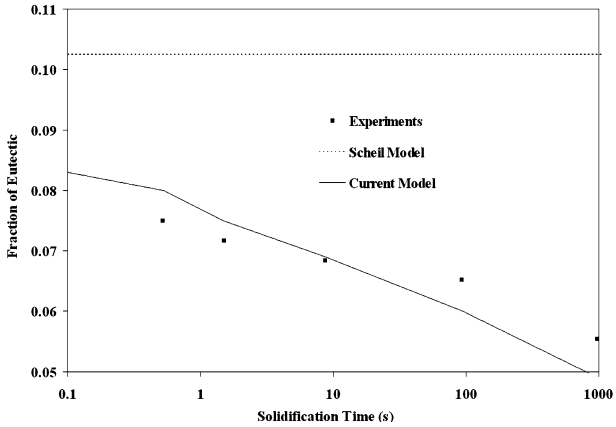

Fig. 2 Eutectic fraction of Al-4.9% Cu alloy with different solidification times

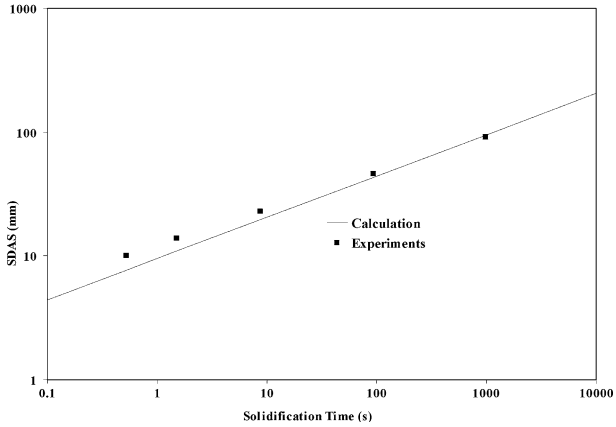

Fig. 3 Secondary dendrite arm spacing

where f_g is the envelope volume divided by the final grain volume.

Please refer to (Ref 19) for details about the derivation of the equations above.

The secondary dendrite arm spacing is calculated by:

$$\lambda_2 = 5.5(Mt_f)^{1/3}, \quad \text{(Eq 9)}$$

where

$$M = \frac{-\Gamma}{\sum_{j=1}^{n} m_j(1-k_j)(c_{e,j} - c_{o,j})/D_j} \cdot \ln\left(\frac{\sum_{j=1}^{n} m_j(1-k_j)c_{e,j}/D_j}{\sum_{j=1}^{n} m_j(1-k_j)c_{o,j}/D_j}\right). \quad \text{(Eq 10)}$$

In order to test the model, a simple binary alloy solidification was performed. Figure 2 shows the predicted eutectic fraction results of solidification of an Al-4.9%Cu alloy compared with experiment (Ref 21). The calculated secondary dendrite arm spacing is shown in Fig. 3. These values are consistent with the experimental measurements (Ref 21).

3. β to α-Phase Transformation for Ti-Based Alloys

For an α + β alloy, the final microstructure after solidification and heat treatment depends strongly on the cooling history from the β region. The β to α-phase transformation follows the classic way to phase transformation. When the alloy is cooled below the β transus temperature, the α-phase is nucleated and grown in plate form starting from β grain boundaries. A final microstructure of globular α is produced if the heat treatment is done in the α-β field. To simplify this complex phenomenon, the α-phase is modeled as globular shape. The classical diffusion model is applied to describe the growth of α-phase. The diffusion rate from the diffusion field around the α-phase determines the growth rate. Fick's second law is applied:

$$\frac{\partial c}{\partial t} = D\nabla^2 c \qquad \text{(Eq 11)}$$

Zener (Ref 22, 23) derived a solution to this diffusion equation for spherical particle growth. The radius is:

$$r = \alpha(Dt)^{1/2}, \qquad \text{(Eq 12)}$$

where α is a growth parameter which is a function of supersaturation.

The diffusivity is calculated by:

$$D = D_o e^{\left(-\frac{Q}{RT}\right)}, \qquad \text{(Eq 13)}$$

where Q is the activation energy.

The grain size of α-phase can be calculated by solving the equations above.

For an isothermal transformation, the well-known Johnson-Mehl-Avrami (JMA) equation can be used to calculate the volume fraction evolution during solid phase transformation with time (Ref 24).

$$f = 1 - \exp[-k(T)t^n], \qquad \text{(Eq 14)}$$

where f is the transformed volume fraction. $k(T)$ is a temperature-dependent coefficient, and n is the Avrami exponent which is usually between 1 and 4. $k(T)$ can be calculated by the formula:

$$k(T) = k_o \exp\left(-\frac{E}{RT}\right), \qquad \text{(Eq 15)}$$

where k_o is a new constant, and E is the activation energy. The fraction of α-phase can then be calculated.

Among the α + β alloys, Ti-6Al-4V is the most popular titanium alloy (Ref 25). Semiatin and coworkers (Ref 26) studied the microstructure evolution during heat treatment of a Ti-6Al-4V alloy. The samples were prepared by furnace heat treatment at 955 °C for 1 h followed by three cooling rates to the room temperature. The volume fractions of α-phase were measured. Figure 4 shows the calculated (lines) fraction of α-phase from the current model. The measured values (symbols) are included for comparison. The agreement between model predictions and measurements is pretty good for all three cooling rates. The grain sizes of α-phase at different temperatures for different cooling rates are shown in Fig. 5.

The fraction of α-phase increases as the temperature reduces for all three cooling rates. The α grain grows very fast at the beginning of the cooling. After that the grain size increases very slowly. This shows the two stages of α formation, growing and coarsening. During the coarsening period, the grain size does not increase much but the fraction of α-phase continues to increase.

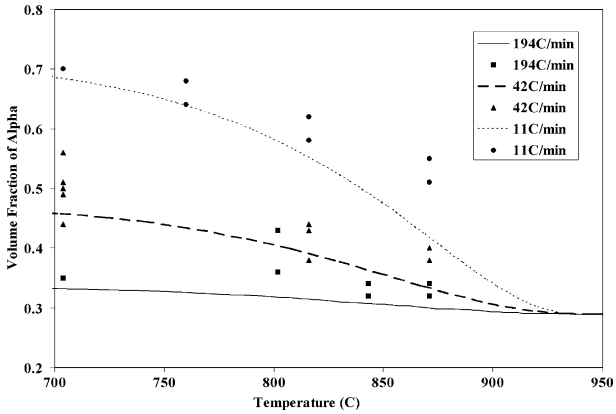

Fig. 4 Comparison of measurements and calculated primary α-phase volume fraction as a function of temperature for different cooling rates

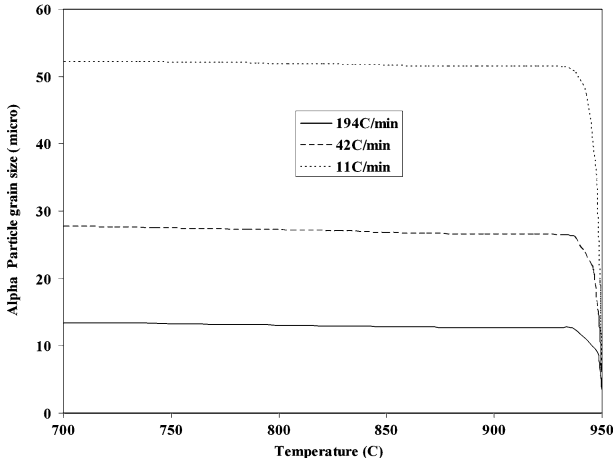

Fig. 5 The average α-phase particle grain size as a function of temperature for different cooling rates

4. Mechanical Properties

The ultimate goal of process modeling is to predict the final mechanical properties. The properties of titanium alloys are primarily determined by the arrangement, volume fraction, and individual properties of the two phases α and β. The yield strength of Ti alloys can be calculated by using the standard Hall-Petch equation (Ref 27) if the alloys are solid solution strengthened, which is the case for many titanium alloys (Ref 28).

$$\sigma_y = \sigma_o + kd^{-1/2}, \qquad \text{(Eq 16)}$$

where σ_y is the yield or proof stress, σ_o is the intrinsic flow stress, k is the Hall-Petch coefficient, and d is the grain size which is calculated from the solidification micromodeling above.

The classical linear law of mixtures can be applied to calculate the total strength since the two phases are reasonably similar.

5. A Study for a Test Casting Part

In order to show the capability of this model, a test casting part is studied. In this study, an investment casting with the composition of Ti-6Al-4V is investigated. A comprehensive multicomponent alloy solidification micro-model, which is coupled with thermal-fluid-stress macro-models, has been developed and implemented in a commercial finite-element analysis software code, ProCAST. The microstructure and the final mechanical properties are predicted. Figure 6 shows the average β-phase dendrite radius in centimeter after solidification. Due to the lower cooling rate in the center of the casting than that on the surface, solidification time in the center is longer. There is less nuclei and more time for β-phase to grow in the center. Hence, the radius of β-phase in the center is larger, which is around 1.0 mm, compared to 0.7 mm on the surface. As the casting cools down to room temperature, some β-phase transforms to α-phase. The fraction of α-phase is shown in Fig. 7. The average particle size in centimeter of the α-phase is calculated and shown in Fig. 8. The transformation depends on the cooling history. Again, the cooling rate is lower in the center of the casting than on the surface for the whole cooling history. This is the reason why there is more α-phase in the center (around 67.5%) than on the surface (around 55%). For the same reason, the grain size of α-phase is slightly larger in the center (~21 micro) than on the surface (~19 micro). There is a relatively longer time for α-phase to grow in the center of the casting. Based on the information of the microstructure and phase fraction, the final yield strength can be predicted. Figure 9 shows the result of the yield strength for this test casting. The yield strength is dependent on the phase volume and the grain size. The stronger part is on the surface of the casting which has maximum yield strength of 895 MPa. The center of the casting is relatively weaker. The yield strength could be as low as 880 MPa. The difference is not large due to the small size of the casting and limited cooling rates across the

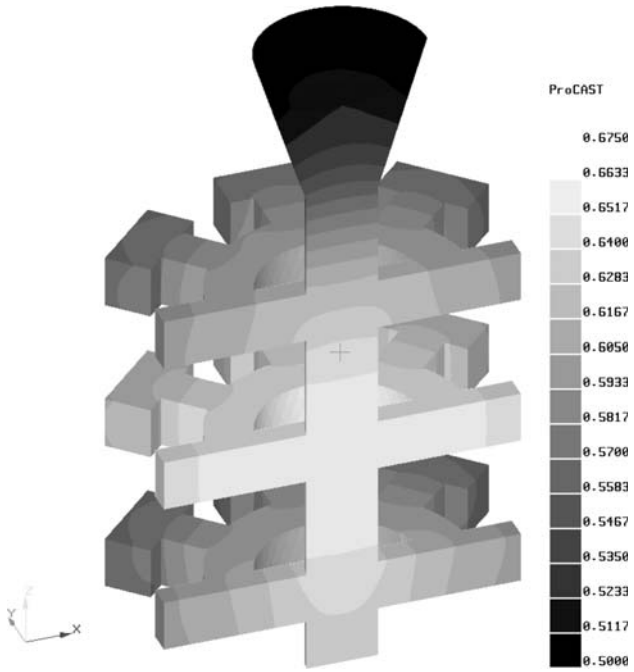

Fig. 7 Fraction of α-phase at room temperature

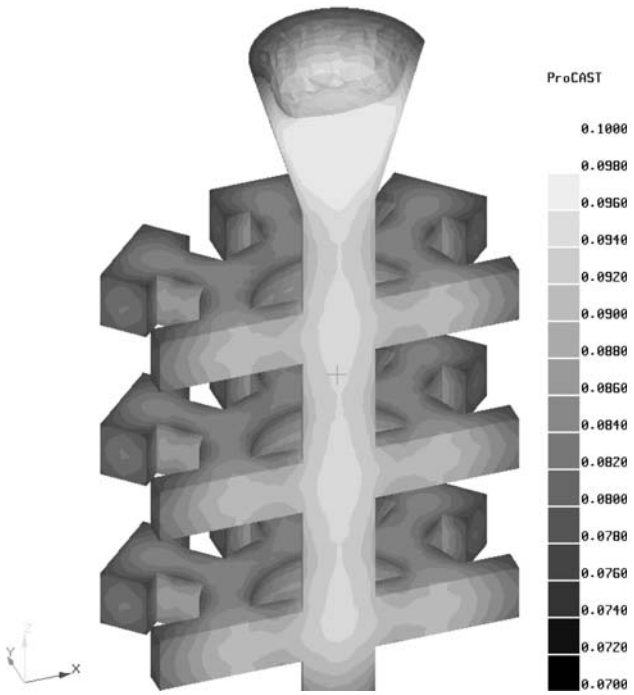

Fig. 6 The average β-phase dendrite radius (cm)

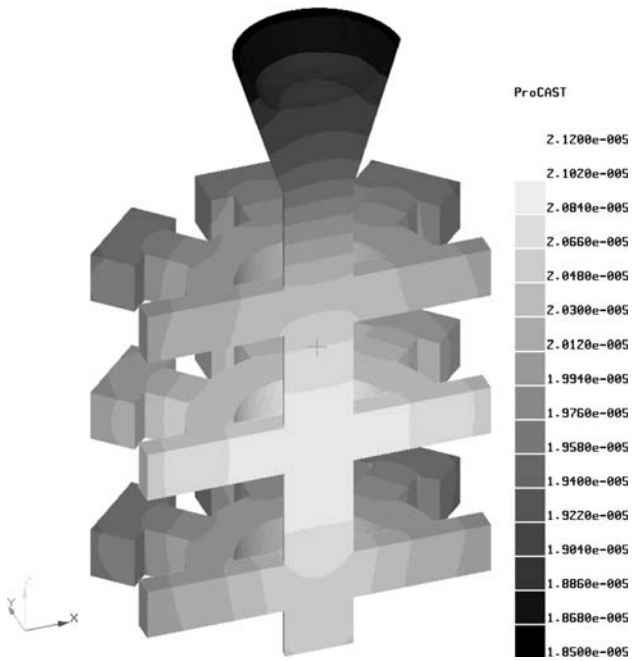

Fig. 8 The average particle size of α-phase (cm)

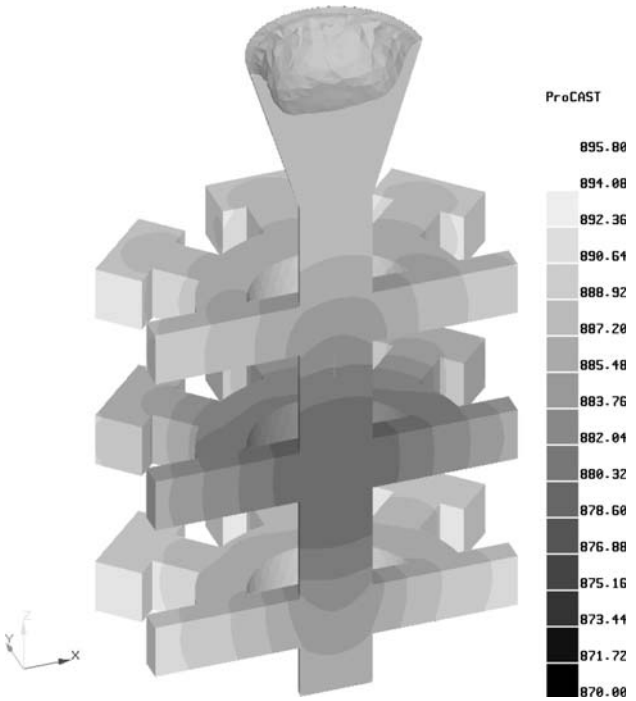

Fig. 9 The yield strength at room temperature (MPa)

casting. Even though the current model can predict the mechanical properties based on the predicted microstructure, it has not yet validated by experimentation.

6. Conclusions

A comprehensive finite-element-based micro-model has been developed to predict the microstructure evolution and the final mechanical properties during titanium alloy β to α-phase transformation. This model can be used for the simulation of casting and heat treatment processes. This model can accurately predict the microstructure and volume fraction of different phases during cooling of a Ti-6Al-4V alloy, as validated by experimental measurements. More experiments are needed to validate the mechanical property predictions.

Acknowledgments

We gratefully acknowledge Dr. Lee Semiatin from the Air Force Research Laboratory, Wright-Patterson Air Force Base, for providing experimental results of the heat treatment of a Ti-6 Al-4 V alloy.

References

1. J. Guo and M. Samonds, Properties Prediction with Coupled Macro-Micromodeling and Computational Thermodynamics, *Modeling of Casting & Solidification Processes 2004*, Hwang Weng-Sing, Ed., Aug 8-11, Metal Industries Research and Development Centre, Kaohsiung, Taiwan, 2004, p157–164
2. I. Katzarov, S. Malinov, and W. Sha, Finite Element Modeling of the Morphology of β to α Phase Transformation in Ti-6Al-4V Alloy, *Metall. Mater. Trans. A*, 2002, **33**, p 1027–1040
3. J. Oh, J.G. Lee, N.J. Kim, S. Lee, and E.W. Lee, Effects of Thinckness on Fatigue Properties of Investment Cast Ti-6Al-4V Alloy Plates, *J. Mater. Sci.*, 2004, **39**, p 587–591
4. A.N. Kalinyuk, N.P. Trigub, V.N. Zamkov, O.M. Ivasishin, P.E. Markovsky, R.V. Teliovich, and S.L. Semiatin, Microstructure, Texture, and Mechanical Properties of Electron-Beam Melted Ti-6Al-4V, *Mater. Sci. Eng. A*, 2003, **346**, p 178–188
5. C.J. Butler, D.G. McCartney, C.J. Small, F.J. Horrocks, and N. Saunders, Solidification Microstructures and Calculated Phase Equilibria in the Ti-Al-Mn System, *Acta Mater.*, 1997, **45**(7), p 2931–2947
6. H.G. Suzuki, E. Takakura, and D. Eylon, Hot Strength and Hot Ductility of Titanium Alloys—A Challenge for Continuous Casting Process, *Mater. Sci. Eng. A*, 1999, **263**, p 230–236
7. A. Mitchell, Melting, Casting and Forging Problems in Titanium Alloys, *Mater. Sci. Eng. A*, 1998, **243**, p 257–262
8. C. Ouchi, H. Fukai, and K. Hasegawa, Microstructural Characteristics and Unique Properties Obtained by Solution Treating or Aging in β-rich α + β Titanium Alloy, *Mater. Sci. Eng. A*, 1999, **263**, p 132–136
9. J. Tiley, T. Searles, E. Lee, S. Kar, R. Banerjee, J.C. Russ, and H.L. Fraser, Quantification of Microstructural Features in α/β Titanium Alloys, *Mater. Sci. Eng. A*, 2004, **372**, p 191–198
10. H. Moustahfid, N. Gey, M. Humbert, and M.J. Philippe, Study of β–α Phase Transformations of a Ti-64 Sheet Induced from a High-Temperature β State and a High-Temperature α + β State, *Metall. Mater. Trans. A*, 1995, **28**, p 51–61
11. H. Fujii, Strengthening of α + β Titanium Alloys by Thermomechanical Processing, *Mater. Sci. Eng. A*, 1998, **243**, p 103–108
12. P.L. Martin, Effect of Hot Working on the Microstructure of Ti-base Alloys, *Mater. Sci. Eng. A*, 1998, **243**, p 25–31
13. T. Seshacharyulu, S.C. Medeiros, W.G. Frazier, and Y.V.R.K. Prasad, Hot Working of Commercial Ti-6Al-4V with an Equiaxed α–β Microstructure: Materials Modeling Considerations, *Mater. Sci. Eng. A*, 2000, **284**, p 184–194
14. S. Nemat-Nasser, W. Guo, V.F. Nesterenko, S.S. Indrakanti, and Y. Gu, Dynamic Response of Conventional and Hot Isostatically Pressed Ti-6Al-4V Alloys: Experiments and Modeling, *Mech. Mater.*, 2001, **33**, p 425–439
15. J. Lindemann and L. Wagner, Microtextural Effects on Mechanical Properties of Duplex Microstructures in (α + β) Titanium Alloys, *Mater. Sci. Eng. A*, 1999, **263**, p 137–141
16. H. Inoue, S. Fukushima, and N. Inakazu, Transformation Textures in Ti-15V-3Cr-3Sn-3Al Alloy Sheets, *Mater. Trans., JIM*, 1992, **33**(2), p 129–137
17. C.J. Boehlert, Microstructure, Creep, and Tensile Behavior of a Ti-12Al-38Nb (at.%) Beta+Orthorhombic Alloy, *Mater. Sci. Eng. A*, 1999, **267**, p 82–98
18. P. Thevoz, J.L. Desbiolles, and M. Rappaz, Modeling of Equiaxed Microstructure Formation in Casting, *Metall. Trans. A*, 1989, **20**, p 311–322
19. M. Rappaz and W.J. Boettinger, On Dendritic Solidification of Multicomponent Alloys with Unequal Liquid Diffusion Coefficients, *Acta Mater.*, 1999, **47**(11), p 3205–3219
20. C.Y. Wang and C. Beckermann, A Multiphase Solute Diffusion Model for Dendritic Alloy Solidification, *Met. Trans. A*, 1993, **24A**, p 2787–2802
21. A. Sarreal and G.J. Abbaschian, The Effect of Solidification Rate on Microsegregation, *Met. Trans. A*, 1986, **17A**, p 2063–2073
22. C. Zener, Theory of Growth of Spherical Precipitates from Solid Solution, *J. Appl. Phys*, 1949, **20**, p 950
23. P.E. Castillo, ''Kinetics of Precipitation Reactions,'' Ph.D. thesis, University of Cambridge, 2002
24. S. Malinov, Z. Guo, W. Sha, and A. Wilson, Differential Scanning Calorimetry Study and Computer Modeling of β⇒α Phase Transformation in a Ti-6Al-4V Alloy, *Metall. Mater. Trans. A*, 2001, **32**, p 879–887
25. C. Leyens and M. Peters, *Titanium and Titanium Alloys*. Wiley-VCH, Weinheim, Germany, 2003
26. S.L. Semiatin, S.L. Knisley, P.N. Fagin, F. Zhang, and D.R. Barker, *Metall. Mater. Trans. A*, 2003, **34**, p 2377–2386
27. E.O. Hall, *Yield Point Phenomena in Metals and Alloys*. Macmillan, London, 1970
28. N. Saunders, X. Li, A. Miodownik, and J. Schille, An Integrated Approach to the Calculation of Materials Properties for Ti-Alloys, *Ti-2003: Proc 10th World Conference on Titanium*, July 13-18, Wiley-VCH, Germany